Urban Climate 28 (2019) 100455

Contents lists available at ScienceDirect

Urban Climate

journal homepage: www.elsevier.com/locate/uclim

Detecting multi-temporal land cover change and land surface temperature in Pearl River Delta by adopting local climate zone

Ran Wang[a], Meng Cai[a,*], Chao Ren[b,c], Benjamin Bechtel[d], Yong Xu[e], Edward Ng[a,b]

[a] School of Architecture, The Chinese University of Hong Kong, Hong Kong Special Administrative Region
[b] Institute of Future Cities, The Chinese University of Hong Kong, Hong Kong Special Administrative Region
[c] Faculty of Architecture, Hong Kong University, Hong Kong Special Administrative Region
[d] Institute of Geography, University of Hamburg, Germany
[e] School of Geographical Sciences, Guangzhou University, China

ARTICLE INFO

Keywords:
Land cover change
World Urban Database and Access Portal Tool (WUDAPT)
Land surface temperature (LST)
Local Climate Zone (LCZ)
Urban Heat Island (UHI) effect

ABSTRACT

This study examines the spatial-temporal changes of land cover and the surface urban heat island (SUHI) effect in the Pearl River Delta (PRD) region from 2000 to 2015. The Local Climate Zone (LCZ) concept is used, given its standard but comprehensive classification scheme designed for urban climate studies. Firstly, historical LCZ maps of the PRD region were generated using the World Urban Database and Access Portal Tools (WUDAPT) protocol. Secondly, summer mean land surface temperature (LST) during daytime and night-time was retrieved from remote sensing data to analyze the SUHI. Thirdly, the correspondence between the spatial-temporal patterns of LCZ and LST were explored. The results show that urbanization in this region comprises transformation from natural land covers to built types and conversion in the built up, in particular densification and vertical enhancement of existing urban types. The LST in the region increased in general but the spatial pattern of LST increase is affected by the land cover change. LCZ 6 (open low-rise) and LCZ 8 (large low-rise) show the greatest increase in LST. LCZ 4 (open high-rise) and LCZ 8 are the two dominant LCZs in high SUHI zone and LCZ 8 keeps growing as the most principal LCZ type.

1. Introduction

Land cover refers to the physical attributes of the surface of the Earth, such as cropland, forest, grasslands, wetlands and so on (Turner et al., 1994; Turner et al., 1993). Due to fast urbanization worldwide, the urban underlying surface changes substantially—most importantly pervious vegetated surfaces transform into impervious surfaces (Mallick et al., 2008). Such land cover changes affect not only the composition of different surface materials but also has effects on flows of substances and energy. The specific influences include changing vegetation types (Yang et al., 2009), land surface emissivity (Gan et al., 2006), surface roughness (Shi et al., 2006), land surface temperature (LST) (Liu et al., 2006), land surface evaporation (Sun and Zhou, 2010), soil quality (Deng et al., 2010), organic matter in water bodies and others (Qin et al., 2010). An intensifying Urban Heat Island (UHI) effect which is closely related to surface changes is seen as an inevitable problem (Mallick et al., 2008). On the one hand, the United Nations project that by 2050, 68% of the world's population will live in urban areas (United Nations, 2018). Moreover, 90% of the growth in urban population will take place in Asia and Africa (United Nations, 2018). Especially, China is projected to add 255 million urban dwellers

* Corresponding author at: School of Architecture, The Chinese University of Hong Kong, Shatin, Hong Kong Special Administrative Region.
E-mail address: caimeng@link.cuhk.edu.hk (M. Cai).

https://doi.org/10.1016/j.uclim.2019.100455
Received 28 June 2018; Received in revised form 27 January 2019; Accepted 19 March 2019

between 2018 and 2050 (United Nations, 2018). On the other hand, the global mean surface temperature during 2006–2015 was observed 0.87 °C higher than that of 1850–1900 (IPCC, 2018). Given the significant urbanization around the world, the surface temperature is expected to keep rising and an increasing proportion of the worldwide population will be exposed to the rising temperature in urban areas (Allen et al., 2014).

The phenomenon that urban temperature is higher than that of its surrounding rural areas, which is called Urban Heat Island (UHI), has been observed and documented worldwide (Clinton and Gong, 2013; Heinl et al., 2015; McCarthy et al., 2010; Oke, 1973; Peng et al., 2011; Santamouris et al., 2015; Zhao et al., 2014). Generally, the UHI comprises both air temperature UHI and surface UHI (SUHI), which are defined by (canopy or boundary layer) air temperature and LST differences between urban and rural areas respectively. Air temperature is measured in situ using station networks. However, the coverage of ground-level observational meteorological stations is limited in China, and air temperature is difficult to acquire in high temporal and spatial resolution. Land surface temperature (LST) measured by thermal infrared radiometers carried by aircraft or satellites can provide continuous coverage, high integrity and real-time data acquisition over large areas (Voogt and Oke, 2003). Thus, the land surface temperature is selected as the focus of this study.

As a consequence of the opening and reform policy which put forward the formation of special economic zones and open cities in coastal areas, the Pearl River Delta (PRD) region has experienced rapid urbanization since 1978 substantially changing the land cover and altering land surface temperature. Many scholars have investigated the changes of land covers, land surface temperature, and surface UHI effect as well as their relationship at a single year or multi-temporal periods in the fast-urbanized PRD region (Chen et al., 2006; Dou and Chen, 2017; Mou and Zhao, 2012; Weng, 2001; Zhang et al., 2007). Scholars particularly focus on the transformation from natural land covers to urban construction types and its impact on land surface temperature in this region (Qian and Ding, 2005; Weng, 2001). However, most studies adopt a rough urban classification scheme with commonly one urban category (Tian et al., 2017). Such a single urban classification system ignores the complexity and spatial heterogeneity of urban structure and does not account for the transformation of the urban structure being the increase in height or density. Detailed urban categories will help develop an in-depth understanding of not only the conversion between natural and urban land cover but also a transformation from one urban type to another. Moreover, the corresponding LST variations will clarify the relationship between land cover changes and the magnitude of the SUHI.

The World Urban Database and Access Portal Tools (WUDAPT) was developed as a new global initiative to produce standardized data on urban form and function for different applications and in different levels of detail (Bechtel et al., 2015; Ching et al., 2018). This most basic description of urban landscapes in WUDAPT (= level zero) (Bechtel et al., 2019a) discretizes urban landscapes into Local Climate Zones (LCZs), a scheme which comprises ten built types and seven land cover types (Stewart and Oke, 2012). With the ten built types, the inner urban structure transformation can be investigated in sufficient details for many climatic applications. Moreover, LCZ links land cover types and urban morphology with corresponding thermal properties, which is particularly suitable for UHI studies (Stewart and Oke, 2012). Thus, we applied the LCZ-based WUDAPT data to detect the changes of land covers and LST in one of the fastest urbanized regions, the PRD region, in China. Researchers have already applied LCZ to SUHI studies at Delhi in India (Budhiraja et al., 2017), Brno and Prague in Czech (Geletič et al., 2016), Szeged in Hungary (Skarbit et al., 2015), Sydney in Australia (Koc et al., 2018), Dubai in the Middle East (Nassar et al., 2016), Taipei in Tai Wan, China (Shih, 2017), Phoenix and Las Vegas in United States (Wang et al., 2018), and Wuhan (Wang et al., 2017), Fuzhou (Lin and Xu, 2016), Yangtze River Delta region in China (Cai et al., 2018). Bechtel et al., 2019b (in press) conducted a SUHI comparison of 50 cities using LCZ. However, on the one hand, the number of the SUHI-LCZ studies is still low at the current stage. On the other hand, due to better data availability from Landsat satellite, the Landsat data are used for SUHI-LCZ studies. Many studies focus only on the daytime situation of SUHI since the Landsat satellite images are only available for daytime. Besides, most of the studies mentioned above merely examined the LST difference between each LCZ class at one day or one year including different seasons but did not investigate the effect of the land cover change. However, the fast urbanization process in the PRD region also allows change analysis within the lifetime of current satellite sensors.

This study employs WUDAPT based LCZ mapping to detect the historical land cover change and relate it to land surface temperature variation in the PRD region. The objectives of this study are to, firstly, apply the WUDAPT method to derive multi-temporal LCZ data and analyze the spatiotemporal changes of land cover and urbanization in the PRD region; secondly, acquire LST distribution pattern and SUHI of this region and identify the general trend of land cover and LST changes; in addition, the LST differences in each LCZ class are explored, and the distribution of LCZ types in each SUHI zone is analyzed; lastly, the LST change of each LCZ class during the study period are compared.

2. Materials and methodology

2.1. Study area

The Pearl River Delta (PRD) region is located in the Guangdong province, in the southeast of China, close to the South China Sea (Fig. 1). The PRD region covers an area of 55,000 km^2. It used to be a major agricultural production area before the implementation of the opening and reform policy in 1978. In the 1980's, the name “Pearl River Delta (PRD) region” was put forward as an economic and industrial region. After the putting forward of the opening and reform policy, with increasing prosperity of different industries, a large population of workers and new immigrants moved into this region. Correspondingly, a large amount of agriculture land was converted into construction land to support economic growth and building construction for urban dwellers. From 2000 to 2010, urban area in the PRD region grew by 2615 km^2 (Statistics Bureau of Guangdong Province, 2001, 2011). In 2008, the urbanization rate of the PRD region was up to 80.5% and the built-up areas took up around 16% of the whole area of the PRD region (Government

Fig. 1. Location and main cities of the Pearl River Delta (PRD) region.

of Guangdong Province, 2010). This leads to rapid land cover change with urban development, a problem that is not unique to the PRD region, since many cities or regions within fast urban development in China. And other fast-developing countries are facing similar problems (Lambin, 1997; Murdiyarso, 2000).

2.2. Data

Images from two satellites were used in this study: Landsat and the Moderate Resolution Imaging Spectroradiometer (MODIS). Landsat data were employed in this study to map LCZ types in the PRD region, due to its long temporal coverage, free availability, and spatial resolution. Landsat 5 images were selected for 1999 and 2009 and Landsat 8 images were selected for 2014, according to their cloud cover and availability (see Table 1). According to the statistics about the urban population and Gross Domestic Product (GDP) in the PRD region in recent decades, the increase rate of both urban population and GDP in this region slowed down during 1999 to 2014 with 2009 serving as the breakpoint. Therefore, land cover change analysis is conducted based on two sub-periods—sub-period 1 (1999–2014) and sub-period 2 (2009–2014).

LST products retrieved from MODIS onboard NASA's Terra satellite were chosen due to several advantages over other remote sensing thermal infrared data (Wan, 2006). Firstly, it has large spatial coverage which can cover the whole PRD region. Secondly, MODIS has a temporal resolution of 0.5 days with passing over the study period twice a day, which captures the surface temperature

Table 1
Landsat images used in this study.

Year	Landsat entity ID	Date of Landsat images
1999	LT51210441999320BKT00	1999-11-16
	LT51210451999320BKT00	1999-11-16
	LT51220441999359BKT00	1999-12-25
	LT51220451999359BKT00	1999-12-25
2009	LT51210442009283BJC00	2009-10-10
	LT51210452009283BJC00	2009-10-10
	LT51220442009306BKT00	2009-11-02
	LT51220452009306BKT00	2009-11-02
2014	LC81210442014281LGN00	2014-10-08
	LC81210452014281LGN00	2014-10-08
	LC81220442014320LGN00	2014-11-16
	LC81220452014320LGN00	2014-11-16

Table 2
LCZ scheme.
Adopted from Stewart and Oke (2012).

LCZ 1: Compact high-rise • Tightly packed buildings with > 10 stories • Little or no green space • Built by concrete, steel, stone and glass	LCZ 2: Compact mid-rise • Tightly packed buildings with three to nine stories • Little or no green space • Built by stone, brick, tile and concrete	LCZ 3: Compact low-rise • Tightly packed buildings with one to three stories • Little or no green space • Built by concrete, steel, stone and glass
LCZ 4: Open high-rise • Openly arranged buildings with > 10 stories • Abundance green space • Built by concrete, steel, stone and glass	LCZ 5: Open mid-rise • Openly arranged buildings with three to nine stories • Abundance of green space • Built by concrete, steel and glass	LCZ 6: Open low-rise • Openly arranged buildings with one to three stories • Abundance of green space • Built by wood, brick, tile and concrete
LCZ 7: Lightweight low-rise • Lightweight building materials with one to two stories • Few or no trees • Land cover is hard-packed	LCZ 8: Large low-rise • Large, openly arranged buildings with one to three stories • Few green spaces • Land cover is mostly paved	LCZ 9: Sparsely built • Sparse arrangement of small or medium-sized buildings in natural setting • Abundance of previous cover
LCZ 10: Heavy industry • Low-rise and mid-rise industrial structures (towers, tanks, stacks) • Few or no trees	LCZ A: Dense trees • Heavily wooded landscape of deciduous and/or evergreen trees	LCZ B: Scattered trees • Lightly wooded landscape of deciduous and/or evergreen trees
LCZ C: Bush, scrub • Open arrangement of bushes, shrubs and short, woody trees	LCZ D: Low plants • Grass or herbaceous plants/crops	LCZ E: Bare rock or paved • Rock or paved cover
LCZ F: Bare soil or sand • Soil or sand cover	LCZ G: Water • Large, open water bodies	

at both daytime and night-time for day-night comparisons. Furthermore, due to its daily temporal resolution, it can provide sufficient data during the study period. Finally, the data is available since 2000, which covers most of the study period. The MODIS LST product is produced using the generalized split-window algorithm (Wan, 2008; Wan and Dozier, 1996). Validation of the LST algorithm showed errors lower than 1 K over homogeneous surfaces such as water, crop, and grassland surfaces (Wan, 2008). Hence, the MODIS Terra global LST and Emissivity 1-day (MOD11A1) data which comprises daytime and night-time LST at 1 km resolution were used in this study (Wan, 2006). The data from June to September for each year were used in this study as the surface urban heat island effect is most pronounced in summer (Zhou et al., 2004).

Since MODIS was only launched in 2000, the MODIS LST data in 2000 was selected as corresponding LST pattern for 1999. In addition, heavy rainfall in the August 2014 caused by a strong typhoon and southwest monsoon in Guangdong province resulted in poor data quality and potential underestimation the summer LST in 2014 (Guangdong Meteorological Service, 2015). Therefore, MODIS data for 2015 instead of 2014 was used in this study. The selected years, 2000, 2009 and 2015, all experienced a hot and generally sunny summer, with summer average air temperatures of 28.5 °C , 29.1 °C and 29.0 °C respectively (Guangzhou Meteorological Service, 2017). To sum up, MOD11A1 data of 2000, 2009, and 2015 were used for LST-LCZ analysis and SUHI analysis in the PRD region. In addition, MOD11A1 data from June to September from every year between 2000 and 2017 were applied for LST trend analysis (Section 3.3.1).

2.3. Method

2.3.1. Local Climate Zone (LCZ) classification

WUDAPT suggests a standardized workflow to generate LCZ maps (Table 2) representing different built and natural land cover types (Bechtel et al., 2015). It contains three major steps: Firstly, the pre-processing of Landsat images: Landsat images were mosaicked into one image to cover the study area. Next, this image was resampled from 30 m to 100 m resolution and clipped to fit the range of the PRD region.

Secondly, selection of training samples: polygons, representing training samples for all LCZ types present were digitized from Google Earth based on local knowledge. In this paper, each LCZ type contains around 100 training samples, selected from Guangzhou, Shenzhen, Zhaoqing, Jiangmen, Zhongshan, Foshan, Dongguan, Zhuhai, Huizhou, Hong Kong, and Macau in the PRD region.

Thirdly, LCZ classification by the random forest classifier: the pre-processed Landsat images and selected training samples were used to train a random forest classifier (Breiman, 2001) using the LCZ classification tool in SAGA (Conrad et al., 2015). Taking advantages of spectral features contained in each training sample, the random forest classifier generated the classification rule and applied it to identify each pixel. The random classifier was selected as an ideal compromise between the achieved accuracy and

computational performance among the previously tested classifiers (Bechtel and Daneke, 2012). Moreover, the classifier is non-parametric, which is essential since each LCZ can have quite different instances or appearances within one city. Also, the random forest provides an unbiased out-of-bag error estimate without requiring additional testing data (Bechtel et al., 2015). This error is the prediction error based on the trees that did not use a specific sample for training and has been widely applied in LST classification. Experimentation with the number of trees in the random forest classifier of 4, 8, 16, 32, 64, 128, and 256 was conducted and the results revealed a flattening out-of-bag error curve at 128 trees, so it was used as the final configuration for the LCZ classifications. Each tree in the classifier is constructed using a sample in which around one-third of the observations are left out. Once all trees are constructed, the resulting class for a given set of inputs is based on majority voting.

Finally, manual corrections were conducted for the historical LCZ maps, which is based on the assumptions that built types do not turn back to natural land cover types. Given the LCZ map of the beginning year 1999 as a reference, the areas identified as built types remain built types in 2009 and 2014.

2.3.2. Change detection

To monitor land development in the PRD region, change detection analysis based on land cover transformation matrices was conducted. This analysis reveals the conversion among different LCZ types during specific periods. The matrix not only contains the exact areas of different LCZs at certain time slot but also indicates the transferred areas of each LCZ type at the beginning and the end of the study period. This transformation information is shown by the matrix (Li and Yeh, 2002) (Eq. (1)).

$$S_{ij} = \begin{bmatrix} S_{11} & S_{12} & \cdots & S_{1n} \\ S_{21} & S_{22} & \cdots & S_{2n} \\ \cdots & \cdots & \cdots & \cdots \\ S_{n1} & S_{n2} & \cdots & S_{nn} \end{bmatrix} \quad (1)$$

In this matrix, n represents the total number of land cover types; i and j represent the land cover type before and after the land cover change, S_{ij} represents the area (m^2) that changed from type i to type j. Values in every row show the transferred areas from land cover type i to different land cover types; values in every column show areas that transferred from different land cover types to land cover type j. The land cover transformation matrix indicates both quantity and direction of land cover change in the study area during a certain period (Deng et al., 2009). It has been commonly used in land cover changing analysis (Li and Yeh, 2002; Liu et al., 2003; Verburg and Overmars, 2009).

2.3.3. Identification of SUHI zones

In this study, the SUHI was analyzed for summer based on averaging the LST data from June to September. This provides a comprehensive representation of summer LST patterns and eliminates short term fluctuations in weather and surface conditions. Thus, the seasonal LST was computed by averaging all available MODIS product in summer in 2000, 2009 and 2015, respectively.

SUHI is often quantified based on a linear urban-to-rural gradient. However, the intra-urban temperature differences in urban areas such as urban green space and urban water landscape can be ignored under this definition (Li et al., 2013; Sun and Chen, 2012). Some studies have used the mean value and the standard deviations of LST in the whole study site to classify different SUHI zones, which can reflect the internal temperature variations in the urban areas (Chen and Yu, 2017; Hu and Brunsell, 2013). Therefore, the SUHI zones classification based on the variation of surface temperature in the entire study area was adopted in this study. Firstly, the LST mean and standard deviation were calculated over the whole of the PRD region. Areas with LST more than one standard deviation above the LST mean were empirically defined as high SUHI zones, and areas with LST less than one standard deviation below the LST mean were defined as low SUHI zones, the medium SUHI zone was defined as the LST value between high and low SUHI zones.

3. Results and discussions

3.1. Land cover change analysis in the PRD region

3.1.1. Overall analysis

The LCZ maps of the PRD region for 1999, 2009 and 2014 are shown in Fig. 2 Accuracy assessment is conducted based on three sets of independent validation samples, which were depicted using Google Earth. The overall accuracies for the LCZ maps of 1999, 2009 and 2014 are 73%, 71%, 76% (Appendix A–C) and the Kappa coefficients for the three maps are 0.70, 0.68 and 0.73 (Appendix A–C). Qualitatively, it is found that the built-up areas in the PRD region kept on enlarging from 1999 to 2014.

Table 3 illustrates the quantitative change of each LCZ type in the PRD region from 1999 to 2014. The results show that the percentage of compact LCZs (LCZ 1–3) keeps rising; while the percentage of open LCZs (LCZ 4–6) decreases slightly between 1999 and 2014. The area of LCZ 7 (lightweight low-rise), most of which are rural villages, reduced over the entire period. The extent of the most natural land cover types, namely LCZ A-G, reduced during the study period.

3.1.2. Land cover transferring analysis

As shown in Table 4, the areas of LCZ built types (LCZ 1–10) increased in sub-period 1. The area of compact LCZ types (LCZ 1–3) increased mainly due to the transformation from other built types and transformation from natural LCZ types, especially LCZ B (scattered trees) and LCZ D (low plants). In this period, the area of LCZ 1 (compact high-rise) doubled by mainly converting from LCZ

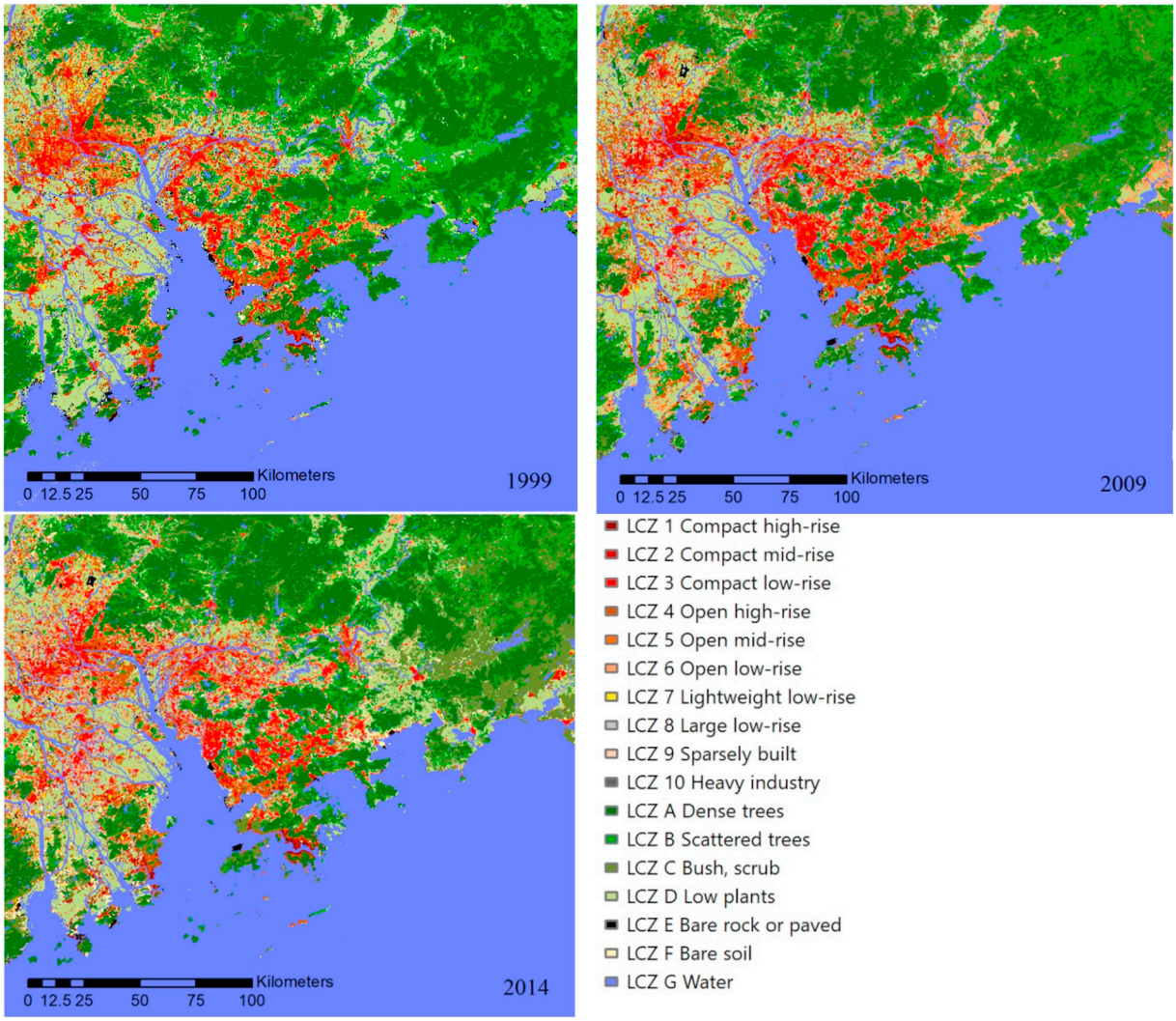

Fig. 2. LCZ maps of the PRD region in the year of 1999, 2009 and 2014.

Table 3
Share of the LCZ types in the PRD region from 1999 to 2014 (%).

Year	1	2	3	4	5	6	7	8	9	10	A	B	C	D	E	F	G
1999	0.21	0.41	1.78	4.87	0.23	2.30	0.52	0.49	0.05	0.12	17.54	11.58	3.23	10.26	0.86	0.57	45.00
2009	0.48	0.32	2.51	6.42	0.16	2.08	0.28	1.92	0.12	0.15	13.38	8.79	8.55	9.41	0.31	0.14	45.00
2014	0.51	0.76	2.70	4.80	0.10	2.06	0.38	2.07	0.22	0.13	14.30	6.51	8.45	9.96	0.43	1.61	45.00

2–5 (compact mid-rise, compact low-rise, open high-rise, open mid-rise). Such conversion illustrates both densification and vertical enhancement in the PRD region. LCZ 4 (open high-rise) enlarged its area by 30% from 1999 to 2009. Apart from natural land cover types, LCZ 6 (open low-rise) contributed to the increase of LCZ 4 (open high-rise), which indicates the vertical enhancement during this period.

For natural LCZ types, transformations mainly occurred between different land covers and from land cover types to built types. LCZ A (dense trees), LCZ B (scattered trees), LCZ C (bush, scrub), and LCZ D (low plants) converted to each other. Noticeably, the area of LCZ A (dense trees) decreased by 2386km^2 with nearly no incoming sources from other LCZ classes, instead, 1566km^2 of LCZ A (dense trees) converted to LCZ B (scattered trees), 628km^2 converted to LCZ C (bush, scrub), and 110km^2 converted to LCZ D (low plants). LCZ B (scattered trees) and LCZ D (low plants) contributed 690km^2 and 990km^2 to the increase of built types (LCZ 1–10), particularly LCZ 1–6 (compact LCZs and open LCZs). For LCZ E (bare rock/paved) and LCZ F (bare soil), both areas decreased during sub-period 1, by 64% and 75%, respectively. While the area of LCZ G (water bodies) remained stable with mere changes of 2km^2.

From 2009 to 2014, sub-period 2 (Table 5), the area of compact LCZs continued to increase but at a slower rate. Except for LCZ 2

Table 4
Land cover transformation matrix of the PRD region from 1999 to 2009 (km^2).

LCZ class		2009																
		1	2	3	4	5	6	7	8	9	10	A	B	C	D	E	F	G	Sum (1999)
1999	1	50	2	13	22	0	8	0	10	1	1	0	1	1	7	1	1	0	120
	2	47	55	85	21	4	2	2	17	0	1	0	0	0	1	1	0	0	237
	3	28	76	599	67	5	44	30	132	1	7	0	1	3	25	5	0	0	1024
	4	40	26	354	1505	27	190	31	322	4	22	7	14	13	216	17	6	0	2795
	5	15	8	14	36	43	4	2	4	0	0	1	0	0	3	0	0	0	130
	6	9	5	136	451	2	210	8	175	18	5	5	51	72	135	26	14	0	1320
	7	2	2	72	39	2	32	68	12	0	0	6	13	7	44	1	0	0	300
	8	2	0	11	43	1	5	1	160	0	0	0	1	2	36	1	0	16	279
	9	0	0	0	4	0	3	0	0	6	0	5	3	4	2	0	0	0	28
	10	1	0	3	18	0	9	0	6	0	19	0	0	1	4	4	0	1	67
	A	3	0	2	94	4	30	0	6	11	1	6701	2058	990	155	7	4	3	10,068
	B	19	1	37	421	1	191	3	85	15	3	491	2392	2318	620	25	22	0	6645
	C	1	0	1	31	0	12	0	3	5	1	362	320	1062	48	2	3	0	1853
	D	47	6	99	742	3	420	12	128	4	10	44	114	342	3881	22	11	1	5888
	E	6	2	12	132	1	24	1	34	0	5	9	11	26	173	56	4	0	496
	F	2	0	2	57	0	11	0	7	1	0	49	63	67	47	5	15	0	326
	G	0	0	0	0	0	0	0	0	0	10	0	1	1	5	3	0	25,811	25,832
	Sum (2009)	273	186	1440	3684	92	1196	158	1100	66	86	7682	5044	4908	5403	175	80	25,834	

*Rows indicate LCZ types in 1999, columns indicate LCZ types in 2009.

Table 5
Land cover transformation matrix of the PRD region from 2009 to 2014 (km^2).

LCZ class		2014																
		1	2	3	4	5	6	7	8	9	10	A	B	C	D	E	F	G	Sum (2009)
2009	1	75	19	16	86	1	5	1	12	0	1	0	1	2	24	4	25	0	273
	2	5	80	54	17	2	3	1	14	0	2	0	0	0	0	6	1	0	186
	3	16	186	841	81	4	46	50	168	2	7	1	5	1	12	13	8	0	1440
	4	110	78	226	1653	18	352	26	195	19	19	37	214	42	466	39	190	0	3684
	5	1	8	5	35	17	15	1	1	0	0	1	2	2	2	1	0	0	92
	6	11	20	112	103	6	289	38	34	13	3	9	57	54	297	31	118	0	1196
	7	1	8	45	10	2	16	62	4	0	0	0	1	1	5	2	2	0	158
	8	12	25	190	80	2	36	3	653	2	9	3	11	3	25	23	21	0	1100
	9	0	0	1	7	0	9	0	1	15	0	5	17	5	4	0	1	0	66
	10	5	2	5	4	0	2	0	18	0	21	0	1	1	1	16	6	4	86
	A	1	0	1	52	0	10	0	2	10	0	6163	591	679	141	2	30	0	7682
	B	1	1	5	78	1	34	2	6	18	1	1143	1538	1567	539	5	105	1	5044
	C	2	1	5	80	0	45	2	7	21	1	757	992	2248	607	4	136	1	4908
	D	42	9	34	451	5	305	26	51	24	6	82	302	237	3572	31	221	5	5403
	E	3	3	8	11	0	8	1	19	0	3	3	2	5	14	64	29	1	175
	F	2	1	2	8	0	5	0	5	0	1	1	7	4	10	4	31	0	80
	G	2	0	0	1	0	0	0	0	0	0	4	0	1	0	4	1	25,821	25,834
	Sum (2014)	290	439	1549	2757	59	1181	216	1190	125	75	8210	3739	4851	5718	249	926	25,834	

*Rows indicate LCZ types in 2009; columns indicate LCZ types in 2014.

(compact mid-rise), the annual increase rate of LCZ 1 (compact high-rise) and LCZ 3 (compact low-rise) slowed down (LCZ 1: 8.60% in sub-period 1, 1.17% in sub-period 2; LCZ 3: 3.47% in sub-period 1, 1.47% in sub-period 2). The major sources for the increase of LCZ 1 (compact high-rise) were still open LCZs and LCZ D (low plants). Different from sub-period 1, the area of LCZ 2 (compact mid-rise) increased by 2.4 times by mainly converting from LCZ 3 (compact low-rise), which also indicates the densification in PRD during this period.

During sub-period 2, except for LCZ B (scattered trees) and LCZ C (bush, scrub), and LCZ G (water bodies), other land cover types increased. While, during sub-period 1, five of the seven land cover types showed a decreasing trend. Despite the continuous transformation from LCZ A-D to LCZ built types, LCZ A (dense trees) and LCZ D (low plants) both gained areas from LCZ B (scattered trees) and LCZ C (bush, scrub). Particularly, compared to no conversion from LCZ B-D during sub-period 1, 553km^2 and 78km^2 of LCZ A (dense trees) converted from LCZ B (scattered trees) and LCZ C (bush, scrub). In addition, different from sub-period 1, areas of LCZ E (bare rock/paved) and LCZ F (bare soil) increased by 1.4 times (74km^2) and 11.6 times (846 km^2), respectively, in sub-period 2. Area of LCZ G (water bodies) also remained stable during this period.

From the above two Tables, the urbanization in the PRD region showed a continuous conversion from natural to urban LCZ types, but also densification as well as and vertical enhancement of existing urban structures. All three processes can clearly be seen in the

Table 6
LST in the PRD region in 2000, 2009 and 2015.

Time	2000	2009	2015
Daytime	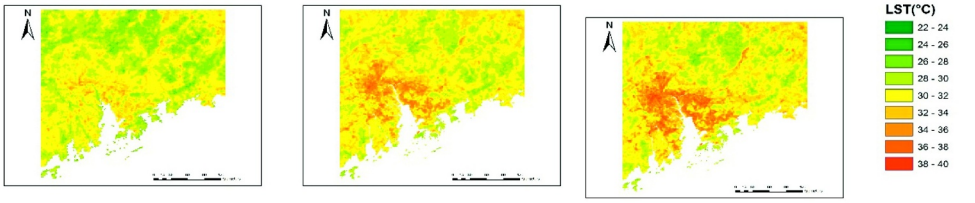		
Night-time	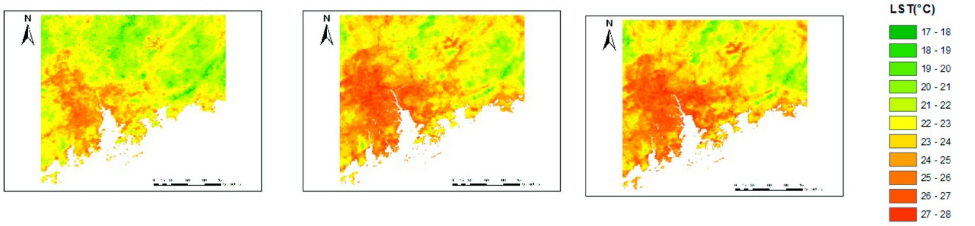		

multi-temporal LCZ mapping.

3.2. Land surface temperature analysis in PRD

Table 6 shows the patterns of LST in the PRD region in 2000, 2009 and 2015, respectively. In general, the higher LST is located in the built-up areas, mainly compromised of the downtown areas of Guangzhou, Dongguan, Foshan, Shenzhen, Hong Kong, Zhuhai, and Macao. In addition, there is no apparent gap of the warmer surface (identified as red in the images) among different cities, indicating the urbanization has led to the built-up areas in different cities merged into one large area. The northeast of the PRD region with less urbanization is also under high LST according to the map.

For the daytime images, there is a significant expansion of areas of high LST value along the coast of Guangzhou, Hong Kong, Macao, Shenzhen, and Zhuhai. Furthermore, significant growth of LST heat intensity is captured from the LST images and the urban areas in 2015 has reached the highest LST in comparison of 2000 and 2009, which may indicate a poor thermal environment in the red areas.

For the night-time situation, the areas with high LST value are not noticeably detected in 2000. However, the night-time image in 2009 identified an obvious increase of LST magnitude in the whole region. The area of high LST value also has large expansion in comparison with the LST in 2000. Also, the night-time LST pattern is different from that of daytime. Higher LST is more significant in the west of the urban areas such as Guangzhou, Foshan, and Zhuhai. The night-time LST pattern in 2015 is similar with that of 2009 during the second period.

Mean and standard deviation (SD) of LST for 2000, 2009 and 2015 and the corresponding LST differences are listed in Table 7. The average summer LST and SD kept growing during the two sub-periods. From 2000 to 2009, the average LST increased by 0.41 °C and 1.62 °C for daytime and night-time. The SD increased from 1.75 to 2.21 during daytime and from 1.41 to 1.58 in the night-time. During the second sub-period of 2000 to 2015, the mean summer LST growth was 0.72 °C and 0.39 °C for daytime and night-time, respectively. The SD also rose from 2.21 to 2.60 in the daytime and from 1.58 to 1.60 in the night-time during the second sub-period.

However, the changes reported in Table 7 represent only discrete points in time and analysis of the LST data each year during the whole period showed that there is substantial inter-annual variation in summer LST. Therefore, trends for the full period were

Table 7
Mean LST, the LST difference and standard deviation of LST in 2000, 2009 and 2015 in the PRD region (°C).

	2000	2009	2015
Average daytime summer LST	30.07	30.48 + 0.41	31.20 + 0.72
Average night summer LST	22.23	23.85 + 1.62	24.24 + 0.39
Standard deviation of daytime summer LST	1.75	2.21	2.60
Standard deviation of night summer LST	1.41	1.58	1.60

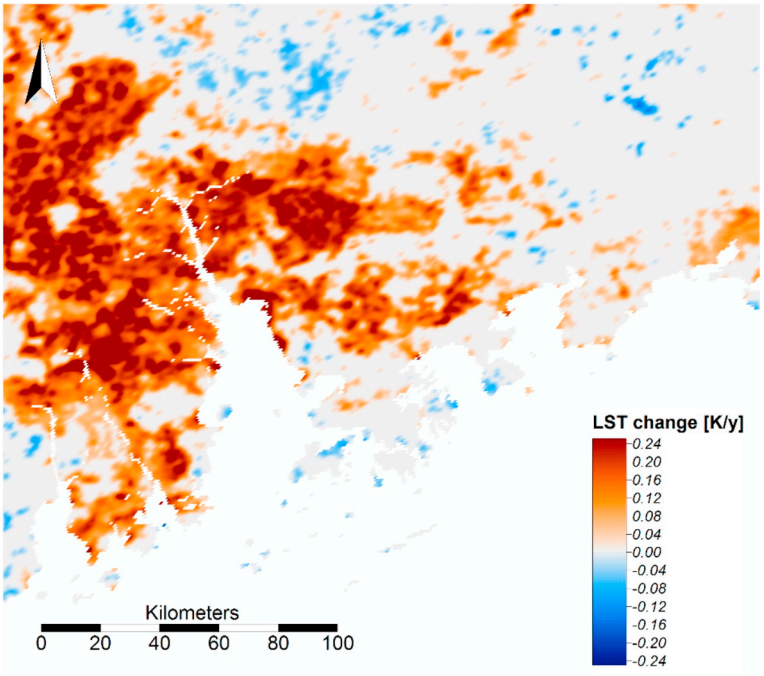

Fig. 3. LST changes from 2000 to 2017 in the PRD region. Grey areas have no significant trends at $\alpha < 0.05$ confidence level.

computed as well.

3.3. Relationship between LST and land cover change

3.3.1. Land surface warming and land LST changes

The land cover changes over the period 1999 to 2014 in the PRD region were compared to LST trends. First, these trends were calculated based on summer average (using all valid acquisitions from June to September) of the daily MODIS data for each year from 2000 to 2017. Then linear trends were derived the time series of annual summer means. Fig. 3 indicates significant LST warming with positive trends of up to > 0.3 K/year for some parts of the PRD region. Only for a few small parts, negative trends are found, grey areas indicate no significant trends at $\alpha < 0.05$. Second, the land cover changes in the PRD region based on historical LCZ maps were reclassified as urbanization (natural turning to built LCZ type), deconstruction (vice versa), static built (same built class in 1999 and 2014), conversion (change within built type), and natural/water (natural class without conversion). This reclassification was needed for a number of reasons, In particular (1) considerable detail of the LCZ scheme with 17 classes technically allows for 272 different conversion (and 17 persistent) types; (2) there is a resolution mismatch between the LCZ and the MODIS data, which means that adjacent conversions have an impact on the LST signal at a point as well. The tends are to be even more problematic than in the static case, since the conversion spots are patchy by nature. Hence, the LCZs were aggregated and only conversions between natural and built types (urbanization), within built types (conversion), as well as unchanged natural and built types were considered. Fig. 4 shows the land cover changes in the PRD region from 1999 to 2014. Finally, a visual comparison was conducted between the LST trends and land cover changes of the PRD region. Both maps match closely, revealing great spatial accordance between the urbanization and conversion (often related to densification or height enhancement) in Fig. 4 and the great LST warming in Fig. 3. Thus, qualitatively, the LST changes clearly echo the land cover changes in the PRD region during the study period and most likely dominantly result from the land cover change.

3.3.2. LST of each LCZ class

To analyze the influence of land cover change on LST, the LST in each LCZ was calculated for daytime and night-time (Fig. 5). It is noted that the mean LST of built types is higher than that of natural LCZ types. Among built types, LCZ 2 (compact mid-rise), 8 (large low-rise), and 10 (heavy industry) have the highest LST values at both daytime and night-time. For natural cover types, LCZ A (dense trees), LCZ B (scattered trees), and LCZ C (bush, scrub) show relatively low mean LST values among all 17 LCZ classes. In addition, variations within the same LCZ class are higher at daytime than at night-time.

LSTs of the majority of the LCZ classes have increased during the two periods, indicating an overall trend of surface warming

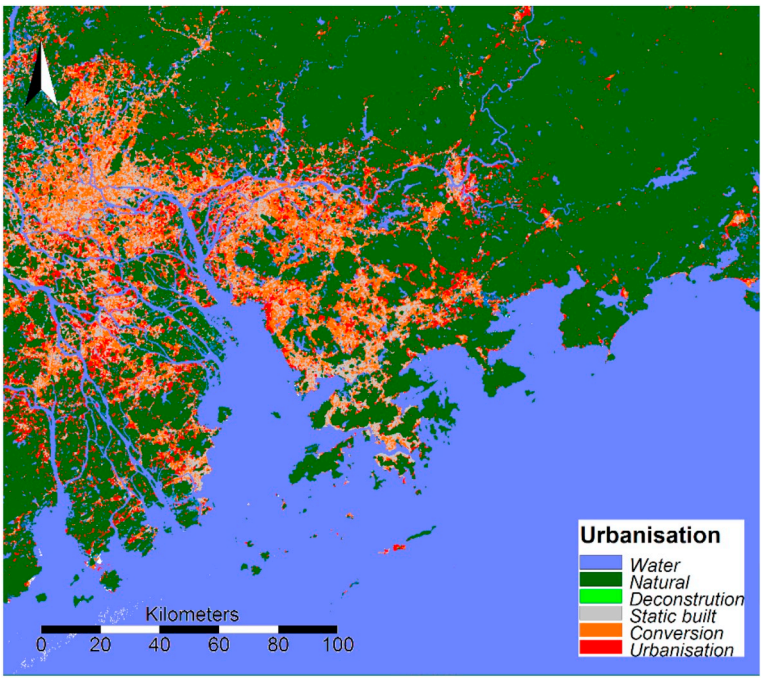

Fig. 4. Land cover changes from 1999 to 2014 in the PRD region

across the study area. However, it also could be related to conversion within one LCZ class or of adjacent patches, since the coarser MODIS data necessarily integrates over somewhat larger areas. In particular, the transformation between different LCZ types (especially urban expansion) has intensified the UHI effect by increasing the LST in the built-up LCZ classes (see Fig. 3). The only LST decrease is identified in LCZ B (scattered trees) from 2000 to 2009. Also, there is a greater increase in the first period than that in the second period.

3.3.3. Dominant LCZ type in SUHI zones

The LSTs have been categorized into SUHI zones and the dominant LCZ type in the SUHI zone has been identified and summarized in Table 8. The low and medium SUHI zones with lower LST are dominated by vegetation and water, i.e. LCZ A (dense trees), LCZ D (low plants) and LCZ G (water). These LCZ types with medium and low SUHI were constant during the 15 years in general, which can result from the low LST and the large areas of these classes.

The high SUHI zone caused by the urbanization process is mainly comprised of two built LCZ types, LCZ 4 (open high-rise) and LCZ 8 (large low-rise), which have large coverage and relatively higher LST among the built types. LCZ 4 (open high-rise) is the principal LCZ type in high SUHI zones in the daytime. The prevailing LCZ type in high SUHI zones in the night has been changed from LCZ 4 (open high-rise) to LCZ 8 (large low-rise) in 2009. The increase of the area of LCZ 8 (large low-rise) which mainly belongs to manufacturing buildings can lead to the increase of the LCZ type in the high SUHI zone. The rapid industrial and urbanization process which can transform land cover types to manufacturing buildings can aggravate the SUHI effect in the PRD region in the future. In addition, the construction of increasing LCZ 4 (open high-rise) can also intensify the SUHI effect in the PRD region.

3.4. Implementation for urban planning

LCZ data produced by WUDAPT are further shown to be effectively and efficiently integrated with land cover change and LST analysis in this study. The spatiotemporal distribution of LCZ can be used for land cover change analysis and LST studies, which are beneficial for understanding urban development, land use planning as well as the thermal environment to minimize the negative impact of urbanization. Rapid urban construction has led to the deterioration of the urban thermal environment; hot spots expanded from several cities into merging city groups. Apart from the positive influence of city group mode on urban development, its adverse impact on the urban thermal environment should also be taken into account, especially for regional planning, such as “The PRD Reform and Development Plan (2008-2020)”. This plan aims to improve the quality of town planning and the management of local urban development through three key aspects: “optimizing spatial plan via making appropriate land use zonings”, “making intensive land use development” and also “conducting environment protection for sustainable development” (National Development and

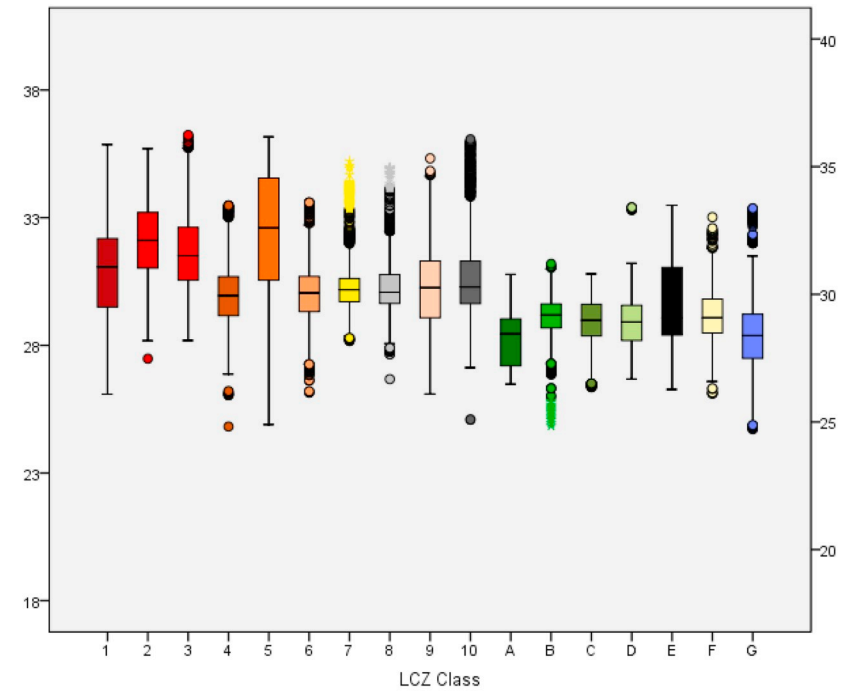

(a) 2000 Daytime

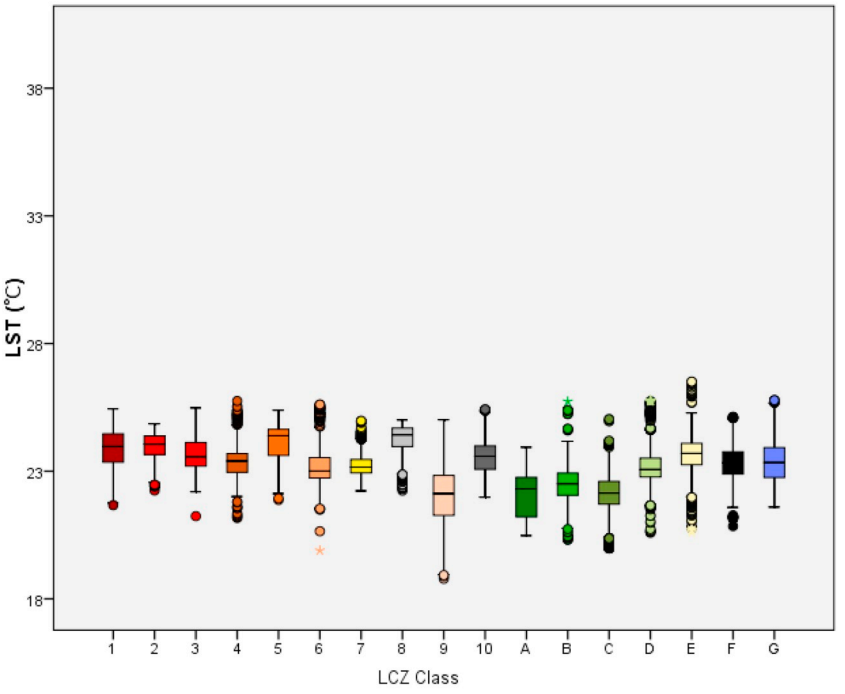

(b) 2000 Night-time

Fig. 5. (a)–(f). LST of each LCZ class during daytime and night-time in 2000, 2009 and 2015.

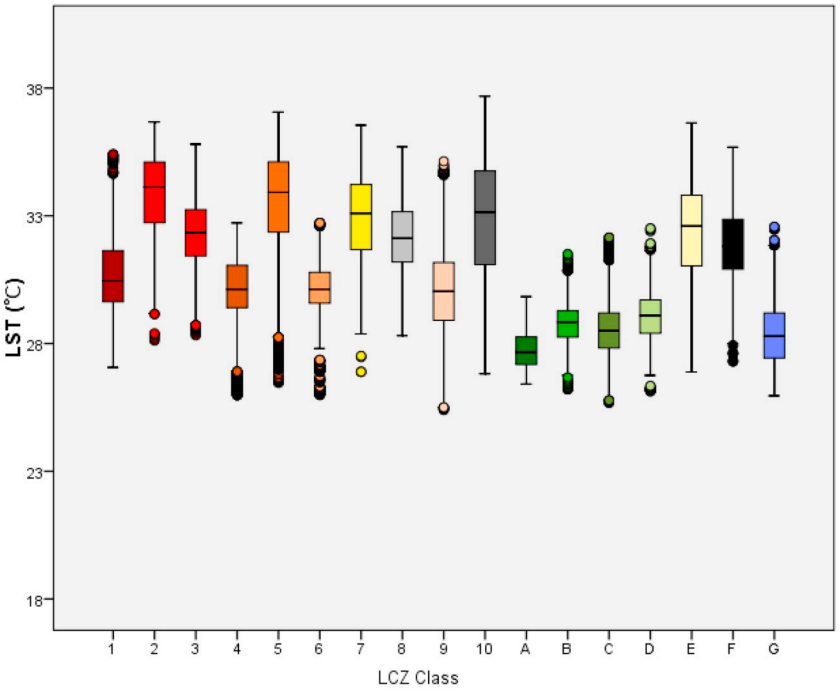

(c) 2009 Daytime

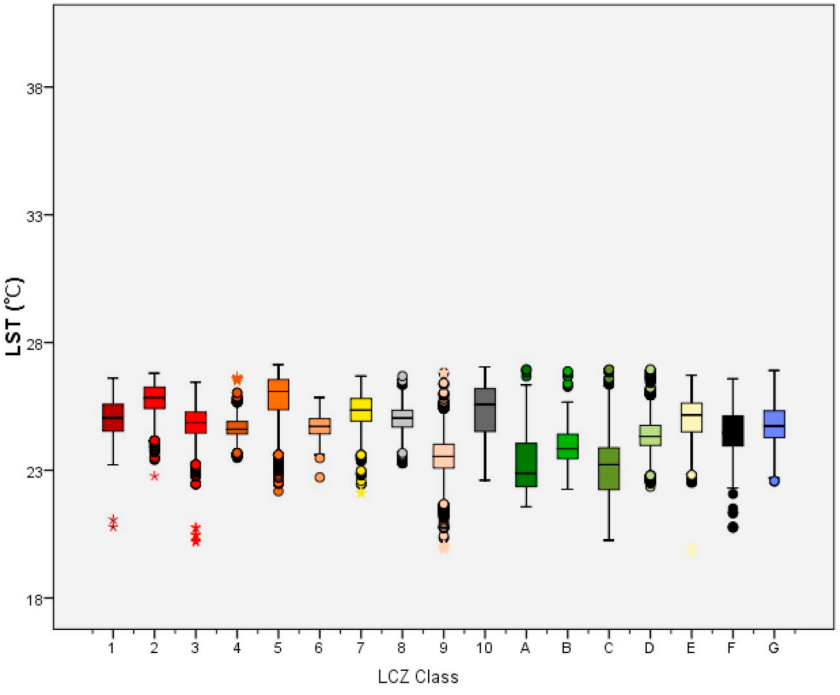

(d) 2009 Night-time

Fig. 5. (*continued*)

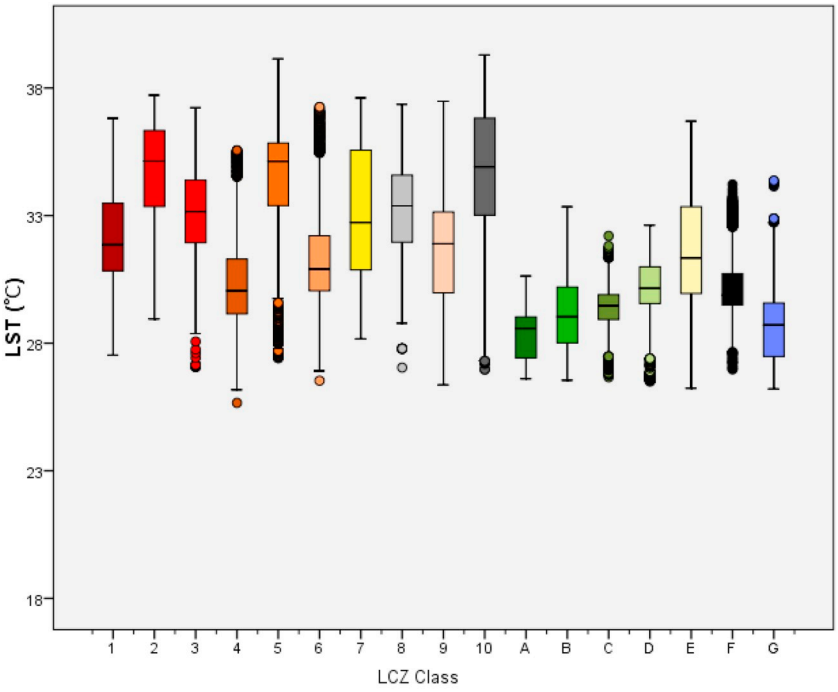

(e) 2015 Daytime

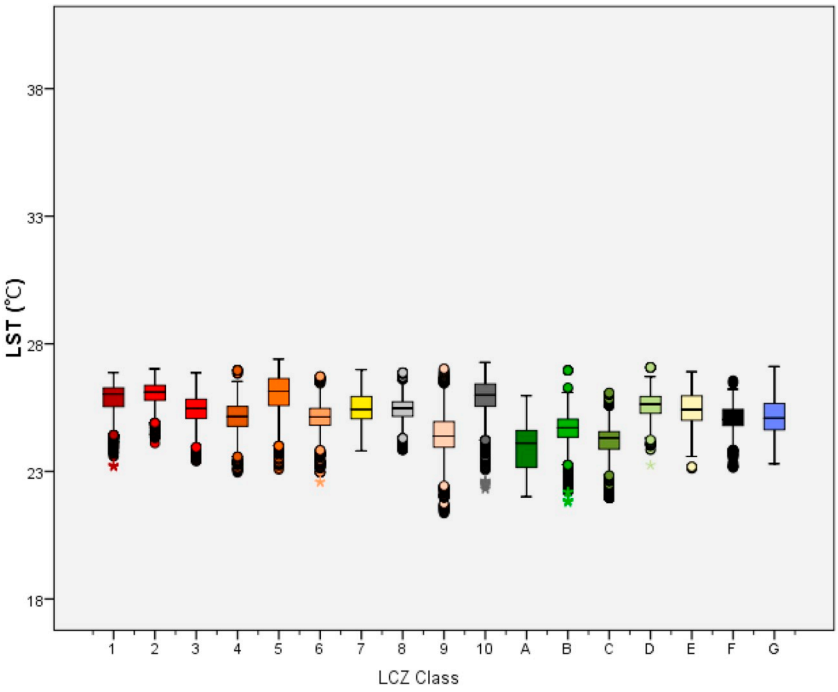

(f) 2015 Night-time

Fig. 5. (*continued*)

Table 8
Dominant LCZ type in SUHI.

Year	Time	Low SUHI	Medium SUHI	High SUHI
2000	daytime	LCZ D (low plants)	LCZ G (water)	LCZ 4 (open high-rise)
	Night-time	LCZ A (dense trees)	LCZ A (dense trees)	LCZ 4 (open high-rise)
2009	daytime	LCZ A (dense trees)	LCZ A (dense trees)	LCZ 4 (open high-rise)
	Night-time	LCZ A (dense trees)	LCZ A (dense trees)	LCZ 8 (large low-rise)
2015	daytime	LCZ A (dense trees)	LCZ A (dense trees)	LCZ 4 (open high-rise)
	Night-time	LCZ A (dense trees)	LCZ A (dense trees)	LCZ 8 (large low-rise)

Reform Commission, 2008). Regarding LCZ classes, in the study period, compact LCZs (LCZ 1–3) were mainly converted from open LCZ types and natural cover types. LCZs with low building height tend to rebuild as LCZ classes with higher heights during the urbanization process. When looking into the thermal environment, LCZ 8 (large low-rise) has the largest increase of LST at daytime, and LCZ 1 (compact high-rise) and LCZ 6 (open low-rise) are the two with the largest increase at night- time (Appendix D). LCZ 4 (open high-rise) and LCZ 8 (large low-rise) also contributed largely to the SUHI in the PRD region. The areas of LCZ 1 (compact high-rise) LCZ 4 (open high-rise), and LCZ 8 (large low-rise) also rose dramatically during this period. Thus, when implementing urban planning for central areas of this mega-urban region, compact LCZ types, particularly compact high-rise types, should be paid more attention, since this type has more impact on the thermal environment. The areas of LCZ 4 (open high-rise) and LCZ 8 (large low-rise) should also be restricted with proper greenery plan in between.

4. Conclusion

Land cover change during the process of urban expansion of the PRD region has relevant influences on local climate spatial patterns, as evidenced by the UHI phenomenon. LCZ mapping and MODIS thermal images were utilized to analyze these processes resulting in the following conclusions. Firstly, a significant change in land cover took place in this area over the 15 years of the study. Urbanization in this region comprises transformation from natural land covers to built types, densification, and vertical enhancement of existing urban structures. Second, the land surface was warming with a speed of up to > 0.3 K/year and hot area expanded in accordance with urbanized areas in the PRD region during the study period. Daytime LST increase is more significant than that of night-time LST. Finally, this warming trend is clearly related to land cover change, in particular, urbanization and conversion between and possibly within LCZ types. The expansion of LCZ built types has led to significant LST increase in these areas. There is some evidence, that in particular the large extension of LCZ 8 (large low-rise) and LCZ 6 (open low-rise) results in high LST increase. LCZ 4 (open high-rise) and LCZ 8 (large low-rise) are the dominant LCZ types in the high SUHI zones. Thus land use planning and management play a crucial role in SUHI reduction. Proper and reasonable distribution of LCZ with lower surface temperatures is advisable to mitigate the influence of UHI during the process of urban development. The findings of this study can also help researchers to better understand the influence of LCZ on local climate variations for other Chinese megaregions. The results will be beneficial to land cover change, and LST comparison studies for cities with different urban context, the latter including the spatial and temporal pattern, their relationship and inner mechanism. In addition, this study also helps provide a deep understanding of the impact of urbanization on LST for urban planners, government officials and researchers. One of the limitations of this study is the quality and resolution of the Landsat and MODIS images. More thermal earth observation missions and further studies are needed to apply higher resolution satellite images to improve the accuracy of the results. Also, there are significant differences between urban air temperature and surface temperature. Urban air temperature acquired from mobile measurement can be helpful to provide more accurate thermal characteristics of different LCZ classes in the future study.

Acknowledgements

This study is supported by the Vice-Chancellor's One-off Discretionary Fund of The Chinese University of Hong Kong titled “World-wide Urban Data Bank on Physical Forms of Cities & Impact Studies of Urban Forms on Human Comfort, Health and Environment Well-being”. It is also supported by a GRF 2016/17 (Project No.: 14643816, named “A study of “Local Climate Zone (LCZ)” of Sub-tropical China's Pearl River Delta (PRD) region by using The WUDAPT method for better Comfortable Living and Sustainable Urban Planning) and RGC Germany/Hong Kong Joint Research Scheme 2016/17 (Ref. No.: G-CUHK411/16; Project Title: Towards Urban Planning Strategies to Improve the Thermal Environment in High Density Cities Based on Better Understanding and Extraction of the Urban Morphology in the WUDAPT Framework)of Hong Kong Research Grants Council. This work was partly supported by the Cluster of Excellence ‘CliSAP’ (EXC177), University of Hamburg, funded through the German Science Foundation (DFG).

Appendix A. Confusion matrix of LCZ map in 1999

LCZ	1	2	3	4	5	6	7	8	9	10	A	B	C	D	E	F	G	No. (GT)	PA (%)
1	48	11	0	2	2	0	0	0	0	0	0	0	0	0	0	0	0	63	76.19
2	3	13	1	2	0	0	0	0	0	0	0	0	0	0	0	0	0	19	68.42
3	0	8	24	4	3	0	3	0	0	0	0	0	0	0	0	0	1	43	55.81
4	0	0	1	47	0	0	0	0	0	0	0	0	0	0	0	0	0	48	97.92
5	0	4	1	16	12	0	0	0	0	0	0	0	0	0	0	0	0	33	36.36
6	0	0	1	14	0	7	0	0	0	0	0	0	0	0	0	0	0	22	31.82
7	0	0	0	6	0	0	5	0	0	0	0	0	0	0	0	0	1	12	41.67
8	0	0	14	51	0	0	0	42	0	0	0	0	0	9	3	0	0	119	35.29
9	0	0	2	0	0	4	0	0	0	0	0	4	0	2	0	0	0	12	0.00
10	6	5	3	2	0	0	0	0	0	10	0	0	0	0	0	0	4	30	33.33
A	0	0	0	0	0	0	0	0	2	0	188	4	11	2	0	0	0	207	90.82
B	0	0	0	6	0	1	0	0	0	0	6	114	2	0	0	0	1	130	87.69
C	0	1	1	0	0	6	0	0	0	0	11	65	66	0	0	6	1	157	42.04
D	0	0	3	7	0	0	0	0	0	0	0	0	0	185	4	0	6	205	90.24
E	0	0	12	5	0	0	0	0	0	1	0	0	0	0	156	2	14	190	82.11
F	0	0	0	10	0	6	0	0	1	0	3	45	0	8	5	57	5	140	40.71
G	0	0	0	0	0	0	0	0	0	0	0	0	0	0	0	0	250	250	100.00
No. (C)	57	42	63	172	17	24	8	42	3	11	208	232	79	206	168	65	283	1680	
UA (%)	84.21	30.95	38.10	27.33	70.59	29.17	62.50	100.00	0.00	90.91	90.38	49.14	83.54	89.81	92.86	87.69	88.34		
OA	73%																		
Kappa	0.70																		

Notes: No. (C) refers to number of classified pixels.
No. (GT) refers to number of ground truth pixels.
UA refers to user's accuracy.
PA refers to producer's accuracy.
OA refers to overall accuracy.

Appendix B. Confusion matrix of LCZ map in 2009

LCZ	1	2	3	4	5	6	7	8	9	10	A	B	C	D	E	F	G	No. (GT)	PA (%)
1	56	1	0	7	2	0	0	0	0	0	0	0	0	0	0	0	0	66	84.85
2	3	22	14	13	0	0	0	5	0	0	0	0	0	1	0	0	0	58	37.93
3	1	0	27	8	2	12	0	0	0	0	0	0	0	0	0	0	0	50	54.00
4	4	0	0	86	0	0	0	0	0	0	0	0	0	0	0	0	4	94	91.49
5	7	0	3	34	7	14	0	0	0	0	0	0	0	0	0	0	0	65	10.77
6	0	0	1	7	0	40	0	1	0	0	0	0	0	2	0	0	7	58	68.97
7	0	0	1	1	1	5	3	0	0	0	0	0	0	6	0	0	0	17	17.65
8	0	0	12	1	0	5	0	93	0	0	0	0	0	0	38	0	1	150	62.00
9	0	0	0	2	0	0	0	0	13	0	4	0	0	10	0	0	0	29	44.83
10	22	1	3	2	0	0	0	10	0	15	0	0	0	0	0	0	5	58	25.86
A	0	0	0	0	0	0	0	0	0	0	189	1	28	24	0	0	0	242	78.10
B	0	0	0	12	0	0	0	1	0	0	0	80	27	3	0	0	2	125	64.00
C	0	0	1	7	0	3	0	5	0	0	7	8	122	1	0	0	1	155	78.71
D	0	0	0	4	0	25	1	0	0	0	0	0	0	152	6	0	17	205	74.15

E	0	14	0	0	0	0	0	2	0	0	0	0	0	0	161	0	38	215	74.88
F	0	0	2	6	0	6	0	7	0	0	0	0	3	0	10	44	0	78	56.41
G	0	0	0	0	0	0	0	0	0	0	0	0	0	0	0	0	250	250	100.00
No. (C)	93	38	64	190	12	110	4	124	13	15	200	89	180	199	215	44	325	1915	
UA (%)	60.22	57.89	42.19	45.26	58.33	36.36	75.00	75.00	100.00	100.00	94.50	89.89	67.78	76.38	74.88	100.00	76.92		
OA	71%																		
Kappa	0.68																		

Notes: No. (C) refers to number of classified pixels.
No. (GT) refers to number of ground truth pixels.
UA refers to user's accuracy.
PA refers to producer's accuracy.
OA refers to overall accuracy.

Appendix C. Confusion matrix of LCZ map in 2014

LCZ	1	2	3	4	5	6	7	8	9	10	A	B	C	D	E	F	G	No. (GT)	PA (%)
1	74	0	0	43	0	0	0	0	0	0	0	0	0	0	0	0	0	117	63.25
2	2	26	24	12	0	0	2	19	0	0	0	0	0	0	0	0	0	85	30.59
3	0	1	40	4	0	0	9	0	0	0	0	0	0	0	4	0	0	58	68.97
4	1	0	0	99	0	0	0	0	0	0	0	0	0	0	0	2	20	122	81.15
5	0	2	7	34	2	15	0	0	0	0	0	0	0	0	0	0	0	60	3.33
6	8	0	2	0	0	74	0	5	0	0	0	0	0	0	0	0	0	89	83.15
7	0	0	2	1	0	6	6	0	0	0	0	0	0	5	0	0	0	20	30.00
8	0	0	4	4	0	3	0	131	0	0	0	0	0	2	17	1	0	162	80.86
9	0	0	0	2	0	3	0	0	23	0	6	4	0	14	0	1	0	53	43.40
10	5	1	2	14	0	0	0	11	0	9	0	0	0	0	0	0	3	45	20.00
A	0	0	1	0	0	2	0	0	0	0	490	22	37	19	0	0	0	571	85.81
B	0	0	0	4	0	3	0	0	0	0	24	100	39	28	0	0	1	199	50.25
C	0	0	0	1	0	5	0	0	0	0	51	21	126	16	0	6	1	227	55.51
D	0	0	0	0	0	20	0	1	0	0	0	0	0	182	0	0	9	212	85.85
E	0	0	2	1	0	0	0	2	0	0	0	0	0	0	174	0	8	187	93.05
F	0	0	0	9	0	0	0	6	0	0	0	0	0	11	1	101	3	131	77.10
G	0	0	0	0	0	0	0	0	0	0	0	0	0	0	0	0	500	500	100.00
No. (C)	90	30	84	228	2	131	17	175	23	9	571	147	202	277	196	111	545	2838	
UA (%)	82.22	86.67	47.62	43.42	100.00	56.49	35.29	74.86	100.00	100.00	85.81	68.03	62.38	65.70	88.78	90.99	91.74		
OA	76%																		
Kappa	0.73																		

Notes: No. (C) refers to number of classified pixels.
No. (GT) refers to number of ground truth pixels.
UA refers to user's accuracy.
PA refers to producer's accuracy.
OA refers to overall accuracy.

Appendix D. Daytime and night-time LST increase in each LCZ (°C) from 2000 to 2015

LCZ	1	2	3	4	5	6	7	8	9	10	A	B	C	D	E	F	G
Daytime	2.58	3.56	3.74	2.8	3.35	2.68	3.45	5.8	2.11	5.07	0.97	1.04	1.14	2.24	4.13	2.64	2.78
Night-time	2.00	1.53	1.53	1.51	1.28	2.04	1.61	1.02	1.84	1.69	1.33	1.28	1.09	1.25	1.58	1.74	1.28

References

Allen, M.R., Barros, V.R., Broome, J., Cramer, W., Christ, R., Church, J.A., ... Edenhofer, O., 2014. IPCC Fifth Assessment Synthesis Report-Climate Change 2014 Synthesis Report.

Bechtel, B., Daneke, C., 2012. Classification of local climate zones based on multiple earth observation data. IEEE J. Sel. Top. Appl. Earth Obs. Remote Sens. 5 (4), 1191.

Bechtel, B., Alexander, P.J., Böhner, J., Ching, J., Conrad, O., Feddema, J., ... Stewart, I., 2015. Mapping local climate zones for a worldwide database of the form and function of cities. ISPRS Int. J. Geo-Info. 4 (1), 199–219.

Bechtel, B., Alexander, P.J., Beck, C., Böhner, J., Brousse, O., Ching, J., ... Xu, Y., 2019a. Generating WUDAPT level 0 data – current status of production and evaluation. Urban Clim. 27, 24–45. https://doi.org/10.1016/j.uclim.2018.10.001.

Bechtel, B., Demuzere, M., Mills, G., Zhan, W., Sismanidis, P., Small, C., Voogt, J.A., 2019b. SUHI analysis using local climate zones. Urban Clim (Accepted).

Breiman, L., 2001. Random forests. Mach. Learn. 45 (1), 5–32.

Budhiraja, B., Pathak, P., Agrawal, G., 2017. Spatio-temporal variability of urban heat islands in local climate zones of Delhi-NCR. In: Paper Presented at the Remote Sensing Technologies and Applications in Urban Environments II.

Cai, M., Ren, C., Xu, Y., Lau, K.K.-L., Wang, R., 2018. Investigating the relationship between local climate zone and land surface temperature using an improved WUDAPT methodology–a case study of Yangtze River Delta, China. Urban Clim. 24, 485–502.

Chen, Y., Yu, S., 2017. Impacts of urban landscape patterns on urban thermal variations in Guangzhou, China. Int. J. Appl. Earth Obs. Geoinf. 54, 65–71.

Chen, X.L., Zhao, H.M., Li, P.X., Yin, Z.Y., 2006. Remote sensing image-based analysis of the relationship between urban heat island and land use/cover changes. Remote Sens. Environ. 104 (2), 133–146. https://doi.org/10.1016/j.rse.2005.11.016.

Ching, J., Mills, G., Bechtel, B., See, L., Feddema, J., Wang, X., ... Neophytou, M., 2018. World Urban Database and Access Portal Tools (WUDAPT), an urban weather, climate and environmental modeling infrastructure for the Anthropocene. Bull. Am. Meteorol. Soc. 2018.

Clinton, N., Gong, P., 2013. MODIS detected surface urban heat islands and sinks: global locations and controls. Remote Sens. Environ. 134, 294–304. https://doi.org/10.1016/j.rse.2013.03.008.

Conrad, O., Bechtel, B., Bock, M., Dietrich, H., Fischer, E., Gerlitz, L., Wehberg, J., Wichmann, V., Böhner, J., 2015. System for automated geoscientific analyses (SAGA) v.2.1.4. Geosci. Model Dev. 8, 1991–2007. https://doi.org/10.5194/gmd-8-1991-2015.

Deng, J.S., Wang, K., Hong, Y., Qi, J.G., 2009. Spatio-temporal dynamics and evolution of land use change and landscape pattern in response to rapid urbanization. Landsc. Urban Plan. 92 (3), 187–198. https://doi.org/10.1016/j.landurbplan.2009.05.001.

Deng, X.Z., Jiang, Q.O., Lin, Y.Z., Han, J.Z., 2010. Simulation of the changes of soil organic carbon stock of cropland in China. Geogr. Res. 29 (1), 93–101.

Dou, P., Chen, Y.B., 2017. Dynamic monitoring of land-use/land-cover change and urban expansion in Shenzhen using Landsat imagery from 1988 to 2015. Int. J. Remote Sens. 38 (19), 5388–5407.

Gan, F.P., Chen, W.T., Zhang, X.J., 2006. The progress in the study of thermal infrared remote sensing for retrieving land surface temperature. Rem. Sens. Land Res. 67 (1), 6–11.

Geletič, J., Lehnert, M., Dobrovolný, P., 2016. Land surface temperature differences within local climate zones, based on two central European cities. Remote Sens. 8 (10), 788.

Government of Guangdong Province, 2010. Pearl River Delta Urban and Rural Integration Planning. Government of Guangdong Province, Guangzhou.

Guangdong Meteorological Service, 2015. Guangdong Meteorology Service Yearbook 2014.

Guangzhou Meteorological Service, 2017. Historical Observational Climatology Data of Guangzhou.

Heinl, M., Hammerle, A., Tappeiner, U., Leitinger, G., 2015. Determinants of urban–rural land surface temperature differences – a landscape scale perspective. Landsc. Urban Plan. 134, 33–42. https://doi.org/10.1016/j.landurbplan.2014.10.003.

Hu, L., Brunsell, N.A., 2013. The impact of temporal aggregation of land surface temperature data for surface urban heat island (SUHI) monitoring. Remote Sens. Environ. 134, 162–174.

IPCC, 2018. Summary for policymakers. In: Global Warming of 1.5°C. World Meteorological Organization, Geneva, Switzerland (33p).

Koc, C.B., Osmond, P., Peters, A., Irger, M., 2018. Understanding land surface temperature differences of local climate zones based on airborne remote sensing data. IEEE J. Sel. Top. Appl. Earth Obs. Rem. Sens. 11 (8), 2724–2730.

Lambin, E.F., 1997. Modelling and monitoring land-cover change processes in tropical regions. Prog. Phys. Geogr. 21 (3), 375–393. https://doi.org/10.1177/030913339702100303.

Li, X., Yeh, A., 2002. Neural-network-based cellular automata for simulating multiple land use changes using GIS. Int. J. Geogr. Inf. Sci. 16 (4), 323–343. https://doi.org/10.1080/13658810210137004.

Li, X., Zhou, W., Ouyang, Z., 2013. Relationship between land surface temperature and spatial pattern of greenspace: what are the effects of spatial resolution? Landsc. Urban Plan. 114, 1–8.

Lin, Z.L., Xu, H.Q., 2016. A study of urban heat island intensity based on "local climate zones": a case study in Fuzhou, China. In: Paper Presented at the Earth Observation and Remote Sensing Applications (EORSA), 2016 4th International Workshop on.

Liu, J.Y., Liu, M.L., Zhuang, D.F., Zhang, Z.X., Deng, X.Z., 2003. Study on spatial pattern of land-use change in China during 1995–2000. Sci. China Ser. D Earth Sci. 46 (4), 373–384. https://doi.org/10.1360/03yd9033.

Liu, Y., Kuang, Y.Q., Wu, Z.F., 2006. Impact of land use on urban land surface temperature-a case study of Dongguan, Guangdong Province. Sci. Geogr. Sin. 26 (6), 602.

Mallick, J., Kant, Y., Bharath, B.D., 2008. Estimation of land surface temperature over Delhi using Landsat-7 ETM+. J. Indian. Geophys. Union 12 (3), 131–140.

McCarthy, M.P., Best, M.J., Betts, R.A., 2010. Climate change in cities due to global warming and urban effects. Geophys. Res. Lett. 37 (9).

Mou, X.J., Zhao, X.Y., 2012. The relationship between land surface temperature and land use in pearl Riverl Delta region. Geogr. Res. 31 (9), 1589–1597.

Murdiyarso, D., 2000. Adaptation to climatic variability and change: Asian perspectives on agriculture and food security. Environ. Monit. Assess. 61 (1), 123–131. https://doi.org/10.1023/a:1006326404156.

Nassar, A.K., Blackburn, G.A., Whyatt, J.D., 2016. Dynamics and controls of urban heat sink and island phenomena in a desert city: development of a local climate zone scheme using remotely-sensed inputs. Int. J. Appl. Earth Obs. Geoinf. 51, 76–90.

Oke, T.R., 1973. City size and the urban heat island. Atmos. Environ. 7 (8), 769–779. https://doi.org/10.1016/0004-6981(73)90140-6.

Peng, S.S., Piao, S.L., Ciais, P., Friedlingstein, P., Ottle, C., Bréon, F.o.-M., ... Myneni, R.B., 2011. Surface urban heat island across 419 global big cities. Environ. Sci. Technol. 46 (2), 696–703.

Qian, L.X., Ding, S.Y., 2005. Impacts of land use and cover change on land surface temperature in the Zhujiang delta. Acta Geograph. Sin. 60 (5).

Qin, H.L., Quan, Z., Liu, X.L., 2010. Phosphorus Status and Risk of Phosphate Leaching Loss from Vegetable Soil of Different Planting Years in Suburbs of Changsha.

China Agriculture Science.
Santamouris, M., Cartalis, C., Synnefa, A., Kolokotsa, D., 2015. On the impact of urban heat island and global warming on the power demand and electricity consumption of buildings—a review. Energy Build. 98, 119–124. https://doi.org/10.1016/j.enbuild.2014.09.052.
Shi, P.J., Wang, J.A., Feng, W.L., Ye, T., Ge, Y., Chen, J., Liu, J., 2006. Response of eco-environmental security to land use/cover change and adjustment of land use policy and pattern in China. Adv. Earth Science 21 (2), 111–119.
Shih, W.Y., 2017. The impact of urban development patterns on thermal distribution in Taipei. In: Paper Presented at the Urban Remote Sensing Event (JURSE), 2017 Joint.
Skarbit, N., Gal, T., Unger, J., 2015. Airborne surface temperature differences of the different local climate zones in the urban area of a medium sized city. In: Paper Presented at the Urban Remote Sensing Event (JURSE), 2015 Joint.
Statistics Bureau of Guangdong Province, 2001. Guangdong Statistical Yearbook. China Statistics, Beijing.
Statistics Bureau of Guangdong Province, 2011. Guangdong Statistical Yearbook. China Statistics, Beijing.
Stewart, I.D., Oke, T.R., 2012. Local climate zones for urban temperature studies. Bull. Am. Meteorol. Soc. 93 (12), 1879–1900. https://doi.org/10.1175/bams-d-11-00019.1.
Sun, R., Chen, L., 2012. How can urban water bodies be designed for climate adaptation? Landsc. Urban Plan. 105 (1–2), 27–33.
Sun, J.S., Zhou, G.S., 2010. Review of advances in measurements and effects of diffuse radiation on terrestrial ecosystem productivity. J. Plant Ecol. 34 (4), 452–461.
Tian, L., Li, Y., Yan, Y., Wang, B., 2017. Measuring urban sprawl and exploring the role planning plays: a shanghai case study. Land Use Policy 67, 426–435.
Turner, B.L., Moss, R.H., Skole, D.L., 1993. Relating land use and global land-cover change. In: Unknown Host Publication Title: International Geosphere-Biosphere Programme, Stockholm; Report, 24/Human Dimensions of Global Environmental Change Programme, Barcelona; Report 5.
Turner, B.L., Meyer, W.B., Skole, D.L., 1994. Global land-use/land-cover change: towards an integrated study. Ambio 23 (1), 91–95.
United Nations, 2018. World Urbanization Prospects: The 2018 Revision. Population Division, Department of Economic and Social Affairs, New York, USA.
Verburg, P.H., Overmars, K.P., 2009. Combining top-down and bottom-up dynamics in land use modeling: exploring the future of abandoned farmlands in Europe with the Dyna-CLUE model. Landsc. Ecol. 24 (9), 1167. https://doi.org/10.1007/s10980-009-9355-7.
Voogt, J.A., Oke, T.R., 2003. Thermal remote sensing of urban climates. Remote Sens. Environ. 86 (3), 370–384. https://doi.org/10.1016/S0034-4257(03)00079-8.
Wan, Z., 2006. MODIS Land Surface Temperature Products Users' Guide. Institute for Computational Earth System Science, University of California, Santa Barbara, CA.
Wan, Z., 2008. New refinements and validation of the MODIS land-surface temperature/emissivity products. Remote Sens. Environ. 112 (1), 59–74.
Wan, Z., Dozier, J., 1996. A generalized split-window algorithm for retrieving land-surface temperature from space. IEEE Trans. Geosci. Remote Sens. 34 (4), 892–905.
Wang, Y.S., Zhan, Q.M., Ouyang, W.L., 2017. Impact of urban climate landscape patterns on land surface temperature in Wuhan, China. Sustainability 9 (10), 1700.
Wang, C.Y., Middel, A., Myint, S.W., Kaplan, S., Brazel, A.J., Lukasczyk, J., 2018. Assessing local climate zones in arid cities: the case of Phoenix, Arizona and Las Vegas, Nevada. ISPRS J. Photogramm. Remote Sens. 141, 59–71.
Weng, Q., 2001. A remote sensing?GIS evaluation of urban expansion and its impact on surface temperature in the Zhujiang Delta, China. Int. J. Remote Sens. 22 (10), 1999–2014. https://doi.org/10.1080/713860788.
Yang, X.C., Zhang, Y.L., Liu, L.S., Zhang, W., Ding, M.J., Wang, Z.F., 2009. Sensitivity of surface air temperature change to land use/cover types in China. Sci. China Ser. D Earth Sci. 52 (8), 1207–1215.
Zhang, J., Wang, Y., Wang, Z., 2007. Change analysis of land surface temperature based on robust statistics in the estuarine area of Pearl River (China) from 1990 to 2000 by Landsat TM/ETM+ data. Int. J. Remote Sens. 28 (10), 2383–2390. https://doi.org/10.1080/01431160701236811.
Zhao, L., Lee, X.H., Smith, R.B., Oleson, K., 2014. Strong contributions of local background climate to urban heat islands. Nature 511 (7508), 216.
Zhou, L., Dickinson, R.E., Tian, Y., Fang, J., Li, Q., Kaufmann, R.K., ... Myneni, R.B., 2004. Evidence for a significant urbanization effect on climate in China. Proc. Natl. Acad. Sci. U. S. A. 101 (26), 9540–9544.